Unveiling stable one-dimensional magnetic solitons in magnetic bilayers

Xin-Wei Jin [1,2] Zhan-Ying Yang,[1,2,*] Zhi-Min Liao [3] Guangyin Jing [1,†] and Wen-Li Yang [2,4]
[1]*School of Physics, Northwest University, Xi'an 710127, China*
[2]*Peng Huanwu Center for Fundamental Theory, Xi'an 710127, China*
[3]*School of Physics, Peking University, Beijing 100871, China*
[4]*Insititute of Physics, Northwest University, Xi'an 710127, China*

(Received 28 June 2023; revised 4 December 2023; accepted 22 December 2023; published 16 January 2024)

We propose a novel model which efficiently describes the magnetization dynamics in a magnetic bilayer system. By applying a particular gauge transformation to the Landau-Lifshitz-Gilbert (LLG) equation, we successfully convert the model into an exactly integrable framework. Thus the obtained analytical solutions allow us to predict a one-dimensional magnetic soliton pair existing by tuning the thickness of the spacing layer between the two ferrimagnetic layers. The decoupling-unlocking-locking transition of soliton motion is determined at various interaction intensity. Our results have implications for the manipulation of magnetic solitons and the design of theoretical magnetic soliton-based distance detection prototype.

DOI: 10.1103/PhysRevB.109.014414

I. INTRODUCTION

The intricate interplay of multiple interactions in magnetic materials generates a large class of localized spin textures—magnetic solitons [1–7]. These solitons exhibit distinct and varied configurations in different dimensions and hold great promise as candidates for the next generation of magnetic storage devices [8,9]. Instead of static magnetic interactions, dynamic magnetic interactions [10–12] have been recently predict and observed by the current-induced torque or nonequilibrium spin pumping [13–19]. Within the dynamic coupling magnetic interaction, two magnets can be coherently and tunable coupled at the macro distance, presenting a novel avenue for the coherent transfer of magnon excitation between distinct magnetic systems [19,20]. Furthermore, these developments raise also an intriguing question of the existence and regulation of attractive magnetic solitons in magnetic bilayer structures [21–23].

Extensive efforts have been dedicated to the quest for stable magnetic solitons in theory, experiments, and micromagnetic simulations [24–29]. Theoretically, the dynamics of magnetic solitons are described by the Landau-Lifshitz-Gilbert (LLG) equation [18,30]. Numerous analytical studies have delved into the original LLG equation that describes single-layer magnets [1,31–36]. As for one-dimensional systems, dynamic multisoliton solutions and topological solitons have been obtained [1,37–40]. These resulting analytical solutions have offered valuable guidance for corresponding experimental and applied research endeavors [41–45]. However, this collaborative synergy between theoretical and experimental work is lacking in multilayer ferromagnetic systems. One significant factor is that the dynamic coupling magnetic interaction not only unveils a host of fresh physical phenomena but also amplifies the complexity of solving the coupled LLG equation from a theoretical standpoint. The lack of comprehensive analytical solutions for the coupled system hinders progress, necessitating time-consuming and labor-intensive experiments and simulations, without the guidance of a solid theoretical framework.

In this paper, we establish an exchange-coupled ferromagnetic/normal/ferromagnetic (F/N/F) bilayer structure as a model system. From the coupled LLG equations governing the magnetization dynamics in the ferromagnetic bilayers, a theoretical model at small amplitude approximation is developed. A gauge transformation is proposed allowing us to convert the problem into an integrable model, which is applicable when the intermediate layer thickness is appropriately chosen. Thereafter, the exact solution of the governing equation is achieved, and the analytical magnetic soliton solutions are subsequently obtained. By adjusting the strength of dynamic magnetic coupling, we find that the magnetic soliton pairs in the ferromagnetic bilayer undergo a decoupled-unlocking-locking transition. We also examine the influence of Gilbert damping in materials on the design of practical devices. These results illustrate practical ways to control the one-dimentional magnetic solitons, in which three motion states are successfully released: antiparallel moving, splitting oscillation, and the locking soliton pair.

II. MODELING

We consider a magnetic bilayer system as illustrated in Fig. 1, which consists of two coupled ferromagnetic (FM) films and a nonmagnetic interlayer with thickness of s. The FM layers are assumed to be parallel to each other with equal thicknesses $d_1 = d_2 = d$. The dynamics of the unit magnetization vector $\mathbf{m}_i$ in the parallel-coupled ferromagnetic layers

*zyyang@nwu.edu.cn
†jing@nwu.edu.cn

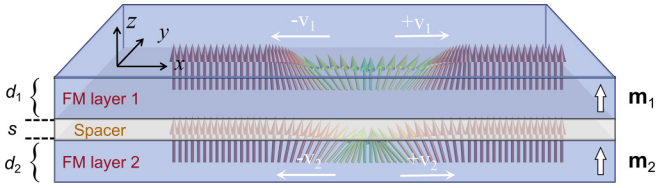

FIG. 1. Sketch of the ferromagnetic/normal/ferromagnetic thin-film bilayer system. The magnetic soliton excitations propagate along x axis. As a reference, the top (bottom) FM layer is labeled $i = 1(i = 2)$. Their corresponding thicknesses are represented by d_1 and d_2, respectively. Parameter s denotes the thickness of the nonmagnetic interlayer.

can be described by the Landau-Lifshitz-Gilbert equation

$$\frac{\partial \mathbf{m}_i}{\partial t} = -\gamma_i \mathbf{m}_i \times \mathbf{H}^i_{\text{eff}} + \alpha_i \left(\mathbf{m}_i \times \frac{\partial \mathbf{m}_i}{\partial t} \right) - \frac{\gamma_i J}{s M_{s,i}} \mathbf{m}_i \times \mathbf{m}_j, \tag{1}$$

where γ_i is the gyromagnetic ratio, $\alpha_i > 0$ denotes Gilbert damping parameter of each FM layer, $M_{s,i}$ is the saturation magnetization, and J represents coupling strength between $\mathbf{m}_i$ and $\mathbf{m}_j$ with $i, j = 1, 2$. We assume magnetic textures vary slowly compared to the spin-coherence length $\lambda_{sc} = \pi/|k_F^{\uparrow} - k_F^{\downarrow}|$ (here $k_F^{\uparrow\downarrow}$ denotes the Fermi-spanning wavevectors), which is smaller than a nanometer for $3d$ metals. Thus the dynamic exchange coupling is considered occurring for $x_1 = x_2$ only. Moreover, the effective field of the two FM layers can be obtained from the free-energy density of the system as $\mathbf{H}^i_{\text{eff}} = -\frac{1}{\mu_0}\frac{\delta E}{\delta \mathbf{m}_i}$. We assume the total energy incorporates the contributions from the Zeeman energy due to an applied magnetic field $\mathbf{H}_0 = (0, 0, h)$, the exchange interaction parametrized by an exchange constant A_i, and the perpendicular magnetic anisotropy energy. Thus, it takes the form $\mathbf{H}^i_{\text{eff}} = \mathbf{H}_0 + (2A_i/M_{s,i})\nabla^2 \mathbf{m}_i + (2K_i/M_{s,i})(\mathbf{m}_i \cdot \mathbf{n})\mathbf{n}$, where $\mathbf{n} = (0, 0, 1)$ is the unit vector directed along the anisotropy axis. We neglect the long-range dipole interaction (this neglect may be justified, e.g., on the assumption $K_i \gg 4\pi$ where the exchange interaction is dominant [1]). For simplicity, we transform the coupled LLG Eq. (1) to the dimensionless form $\frac{\partial \mathbf{m}_i}{\partial \tau} = -\mathbf{m}_i \times \frac{\partial^2}{\partial \zeta^2}\mathbf{m}_i - \kappa \mathbf{m}_i \times (\mathbf{m}_i \cdot \mathbf{n})\mathbf{n} - J' \mathbf{m}_i \times \mathbf{m}_j$, by rescaling the space and time into $\zeta = \lambda_{ex}^{-1} \cdot x$, $\tau = \gamma \mu_0 M_s \cdot t$. Here $\lambda_{ex} = \sqrt{2A_i/(\mu_0 M_{s,i}^2)}$ is the exchange length, and $\kappa = 2K_i/(\mu_0 M_{s,i}^2)$ and $J' = J/(\mu_0 s M_{s,i}^2)$ denote the dimensionless easy-axis anisotropy constant and dimensionless coupling strength, respectively. Table I summarizes the realistic physical constants and parameters used for the structure under our consideration.

TABLE I. The physical constants and parameters used.

Physical constants/parameters	Symbol	Value	Unit
Gyromagnetic ratio	γ	1.76×10^{11}	$\frac{\text{rad}}{\text{s}\cdot\text{T}}$
Saturation magnetization	M_s	5.8×10^5	$\frac{\text{A}}{\text{m}}$
Exchange stiffness	A	1.3×10^{-11}	$\frac{\text{J}}{\text{m}}$
Magnetic anisotropy	K	5×10^5	$\frac{\text{J}}{\text{m}^3}$
Magnetic permeability in vacuum	μ_0	$4\pi \times 10^{-7}$	$\frac{\text{H}}{\text{m}}$
Damping parameter	α	$0.01 \sim 0.05$	

While the original Landau-Lifshitz equation in one dimension is integrable, the integrability of the coupled Landau-Lifshitz equation that describes magnetic bilayer systems remains an open question. Take into account the fact that the magnitude of the magnetization $\mathbf{m}_i^2 = 1$ at temperature well below the Curie temperature, we reasonably introduce a stereographic transformation $\Phi_j = m_j^x + i m_j^y$, $(m_j^z)^2 = 1 - |\Phi_j|^2$. Furthermore, let us consider small deviations of magnetization $\mathbf{m}_i$ from the equilibrium direction (along the anisotropy axis), which corresponds to $(m_j^x)^2 + (m_j^y)^2 \ll (m_j^z)^2$ (or $|\Phi_j|^2 \ll 1$) and therefore $m_j^z \approx 1 - |\Phi_j|^2/2$. As a result, neglecting the Gilbert damping, the dynamics of the variables $\mathbf{\Phi} = (\Phi_1, \Phi_2)^T$ can be expressed as

$$i\Phi_{1\tau} - 2a\Phi_{1\zeta\zeta} - \left(\kappa|\Phi_1|^2 + \frac{J'}{2}|\Phi_2|^2\right)\Phi_1 + \Delta\Phi_1 - J'\Phi_2 = 0, \tag{2a}$$

$$i\Phi_{2\tau} - 2a\Phi_{2\zeta\zeta} - \left(\frac{J'}{2}|\Phi_1|^2 + \kappa|\Phi_2|^2\right)\Phi_2 + \Delta\Phi_2 - J'\Phi_1 = 0, \tag{2b}$$

where $a = A_i$, $\Delta = J' + h + 2\kappa$. The significant observation in this paper is that by maintaining a certain separation between two ferromagnetic layers ($s = J/2K$), for the Co/Cu/Co structure, the value of the thickness of the nonmagnetic layer is about 2 nm, it becomes possible to introduce a gauge transformation $\Phi_{1,2} = \frac{1}{\sqrt{2}}(\Psi_1 e^{i(h+2\kappa)\tau} \pm \Psi_2 e^{i(h+6\kappa)\tau})$, to transform the dynamic model Eq. (1) into an integrable frame in absence of damping. Finally, Eqs. (2) are transformed into the Manakov equation with arbitrary constant coefficients:

$$i\Psi_{1\tau} - 2a\Psi_{1\zeta\zeta} - \kappa(|\Psi_1|^2 + |\Psi_2|^2)\Psi_1 = 0, \tag{3a}$$

$$i\Psi_{2\tau} - 2a\Psi_{2\zeta\zeta} - \kappa(|\Psi_2|^2 + |\Psi_1|^2)\Psi_2 = 0. \tag{3b}$$

Numerous solutions of this equation can be constructed using the methods of exactly integrable systems. Then, one can also easily obtain the formulations of three components of magnetization by the inverse transformation from Eqs. (2).

III. RESULTS

A. Magnetic soliton solutions

Inspired by the nondegenerate optical solitions proposed by S. Stain *et al.* [46] in Manakov systems, here we obtained the new type of soltions in magnetic system, which is absent in theoretical predictions for magnetic materials. In this context, *degenerate* means that the fundamental soliton nature is characterized by a single wave number in all the components. From an applied perspective, the multihump characteristics of nondegenerate solitons will serve to enhance data flow in magnetic transmission applications. On the other hand, the energy-sharing collision properties of degenerate magnetic solitons also hold the potential for constructing logic gates and applying them in spintronic electronic switching devices.

The nondegenerate magnetic soliton solutions of Eq. (3) can be constructed with the help of the Hirota bilinear formalism [46–48] and Darboux transformation [49]. Here, the

exact first-order nondegenerate soliton solution reads (see Supplemental Materials [50] for detailed derivation of first- and second-order nondegenerate magnetic solitons)

$$\Psi_1 = \frac{\alpha_{11}e^{\eta_1} + \Delta_{11}e^{\eta_1+\xi_1+\xi_1^*}}{1+\delta_1 e^{\eta_1+\eta_1^*}+\delta_2 e^{\xi_1+\xi_1^*}+\delta_{11}e^{\eta_1+\eta_1^*+\xi_1+\xi_1^*}},$$
$$\Psi_2 = \frac{\alpha_{12}e^{\xi_1} + \Delta_{12}e^{\xi_1+\eta_1+\eta_1^*}}{1+\delta_1 e^{\eta_1+\eta_1^*}+\delta_2 e^{\xi_1+\xi_1^*}+\delta_{11}e^{\eta_1+\eta_1^*+\xi_1+\xi_1^*}}, \quad (4)$$

with

$$\delta_1 = \frac{\kappa|\alpha_{11}|^2}{4a(k_1+k_1^*)^2},\ \Delta_{11} = \frac{\kappa\alpha_{11}|\alpha_{12}|^2(k_1-l_1)}{4a(l_1+l_1^*)^2(k_1+l_1^*)},$$
$$\delta_2 = \frac{\kappa|\alpha_{12}|^2}{4a(l_1+l_1^*)^2},\ \Delta_{12} = \frac{-\kappa\alpha_{12}|\alpha_{11}|^2(k_1-l_1)}{4a(l_1+l_1^*)^2(k_1^*+l_1)},$$
$$\delta_{11} = \frac{\delta_1\delta_2(k_1-l_1)(k_1^*-l_1^*)}{(k_1+l_1^*)(k_1^*+l_1)}. \quad (5)$$

Here $\eta_1 = k_1\zeta - 2iak_1^2\tau$ and $\xi_1 = l_1\zeta - 2ial_1^2\tau$ are the traveling wave forms of each solitary wave. This first-order nondegenerate soliton solutions are characterized by four arbitrary complex parameters, describing the velocity and the amplitude of the magnetic soliton in both FM layers, as well as the nonlinear interaction of magnetic solitons between two FM layers.

The derived solutions Eq. (4) represent several categories of magnetic solitons in this magnetic bilayer system. In particular, in the special case when $k_1 = l_1$, the nondegenerate soliton solution Eq. (4) degenerates into the standard bright soliton form

$$\Psi_i = \frac{\alpha_{1i}e^{\eta_1}}{1+e^{\eta_1+\eta_1^*+R}},\quad i=1,2, \quad (6)$$

where $e^R = \kappa(|\alpha_{11}|^2+|\alpha_{12}|^2)/[4a(k_1+k_1^*)^2]$. Through analyzing all these solutions, it becomes apparent that the magnetic bilayer system possesses diverse spin textures, manifested as dynamical magnetic solitons. With this theoretical prediction, in the following, we try to discuss the possible generation mechanisms and the practical applications by these magnetic soliton pairs in magnetic bilayer structures.

B. Linear stability analysis

It has been confirmed that, from the analytical solution above, there are magnetic solitons allowed in this system, then another important aspect to be considered is their stability characters. For practical applications of magnetic solitons as memory units or driven objects in spintronics, it is crucial to maintain stability of solitons in the presence of interference. The stability property is usually analyzed by way of linear stability analysis [51–53]. For this purpose, we consider the solitary wave solutions of the form $\Psi_{1,2} = \Psi'_{1,2}\exp(ib\tau)$, with b being propagation constant, then Eq. (5) becomes

$$-b\Psi'_{1\tau} - 2a\Psi'_{1\zeta\zeta} - \kappa(|\Psi'_1|^2+|\Psi'_2|^2)\Psi'_1 = 0, \quad (7a)$$

$$-b\Psi'_{2\tau} - 2a\Psi'_{2\zeta\zeta} - \kappa(|\Psi'_2|^2+|\Psi'_1|^2)\Psi'_2 = 0. \quad (7b)$$

To analyze the linear stability of the solitary wave, we perturb the relevant wavefunction as $\Psi_i = \{\Psi'_{0i} + [v_i(\zeta)+w_i(\zeta)]e^{\lambda\tau} + [v_i^*(\zeta)-w_i^*(\zeta)]e^{\lambda^*\tau}\}e^{ib\tau}$, here Ψ'_{0i} being the general complex-valued unperturbed wavefunction calculated from Eq. (3), v_i and $w_i (i=1,2)$ are small perturbations for a given eigenvalue λ. Inserting this perturbed solution in Eq. (3) and linearizing thereafter, we obtain the following linear-stability eigenvalue problem:

$$i\mathbf{L}\cdot\mathbf{W} = \lambda\cdot\mathbf{W}, \quad (8)$$

where matrix $\mathbf{W} = (v_1, w_1, v_2, w_2)^{\mathrm{T}}$ denotes the normal-mode perturbations. The matrix $\mathbf{L}$ contains the magnetic soliton solution Ψ'_{0i} representing the linear stability operator. The matrix elements and calculation details of matrix $\mathbf{L}$ are presented in Supplemental Materials [50].

In general, two separate regions can be defined based on the linear-stability spectrum. The nondegenerate soliton wave is linearly unstable when the spectrum contains eigenvalues with positive real parts, which gives an exponential growth rate of perturbations. While the linear spectrum of the soliton solution is regarded as stable if the spectrum contains purely imaginary discrete eigenvalues [51]. It is noteworthy that delving into the subtleties of the applicability of linear approximations calls for the use of the renowned Lyapunov criterion [54]. The whole spectrum of the linear-stability operator $\mathbf{L}$ are numerically solved by the Fourier collocation method.

To verify the predictions of the linear stability analysis obtained from the numerical solution of the spectral problem Eq. (7), we proceed to numerically simulate the nonlinear propagation of the magnetic solitons. The evolutions of stable nondegenerate magnetic solitons and unstable nondegenerate magnetic solitons are illustrated in Fig. 2. The initial conditions for both simulations are taken in the form of a soliton solution perturbed by a 10% random noise. The upper panels of Fig. 2(a) depict the stability regions in the parameter space $[\mathrm{Im}(k_1), \mathrm{Re}(l_1)]$ of the magnetic soliton and provide an exemplary illustration of a stable soliton solution. The center panel plots the shape of m^z component in two ferromagnetic layers at $t=0$ and $t=30$. The whole stability spectrum of this nondegenerate soliton is shown in the upper-right corner panel. It can be seen that this flat-bottom-double-hump magnetic solitons propagates stably and the flat-bottom structure in the first FM layer is maintained, which complies with the results of the linear stability analysis. On the other hand, Fig. 2(b) shows the unstable propagation of the asymmetric single-double-hump soliton. Stronger instabilities cause the splitting and diffusion of the solitons at relatively short times. We also conducted numerical simulations of 2D perturbation propagation of magnetic solitons in finite-width bilayer thin films. The results align with the predictions from linear stability analysis, and these findings are presented in the Appendix.

C. Coupling and Gilbert-damping

The successful stabilization of magnetic soliton pairs enlightens us to design potential magnetic soliton-based spintronic devices. In what follows, we chose degenerate magnetic solitons as our test subjects for two reasons: Firstly, degenerate solitons have simpler profiles, providing convenience for experimentally generating magnetic solitons through local external magnetic fields. Secondly, degenerate magnetic solitons exhibit enhanced resistance to external noise. Here, we numerically investigate the propagation behavior of

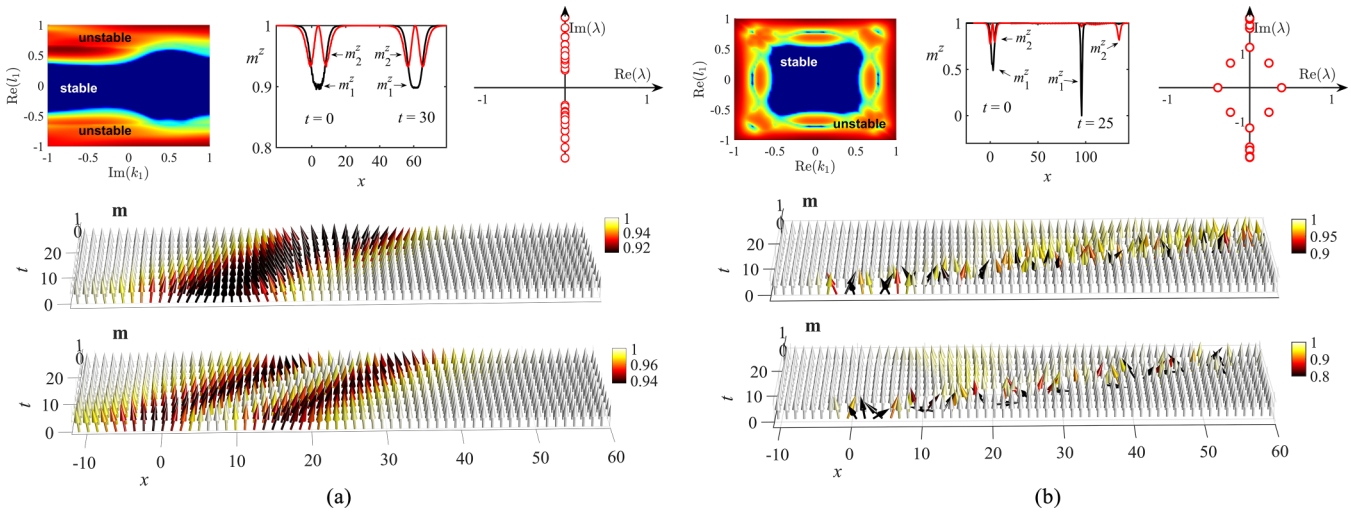

FIG. 2. Propagations of stable and unstable nondegenerate magnetic solitons. (a) Left panel: Stability regions in the parameter space [Im(k_1), Re(l_1)]. Center panel: m^z profiles of symmetric flat-bottom-double-hump magnetic soliton at $t = 0$ and $t = 30$. Right panel: eigenvalue spectrum. Bottom panel: stable propagations of magnetic soliton in two FM layers. (b) Left panel: Stability regions in the parameter space [Re(k_1), Re(l_1)]. Center panel: m^z profiles of asymmetric double-hump-double-hump magnetic soliton at $t = 0$ and $t = 30$. Right panel: eigenvalue spectrum. Bottom panel: unstable propagations of magnetic soliton in two FM layers.

stable magnetic solitons in FM bilayers with various coupling strengths (which corresponds to thickness of the nonmagnetic spacer).

Our first step is to construct a stable magnetic soliton in each layer, with opposing velocities. When the two ferromagnetic layers are far apart from each other, their interaction becomes very weak, and the two layers are decoupling ($J' = 0$). In this situation, the magnetic solitons are governed by two separate scalar nonlinear Schrödinger (NLS) equations. In other words, the initial state in this case consists of two independent scalar magnetic solitons. The two solitons propagate in opposite directions respectively, as depicted in Figs. 3(a) and 3(b). As the two magnetic layers approach each other, the magnetic solitons start to couple, transitioning into the unlocking region. Magnetic solitons within two magnetized layers, possessing opposing momenta, mutually attract one another and exhibit a propensity to draw in the other toward their respective directions [as shown in Figs. 3(c) and 3(d)]. This observation can be explained as follows. As the thickness of the intermediate layer reduces, the long-range dynamic interaction between the two FM layers, induced by adiabatic spin pump, starts to come into play. The dynamic magnetization, which arises from the moving magnetic solitons in the ferromagnetic layer, causes the formation of nonequilibrium spin flow between the two layers. This interlayer dynamic coupling vies with the Heisenberg exchange interaction within the layers, culminating in the emergence of two oscillatory branches of magnetic solitons within each layer. Each branch bears a share of energy, as depicted in Figs. 3(c) and 3(d). The energy ratio between these two branches is correlated with the intensity of the coupling interaction. We highlight that as the two ferromagnetic layers continue to approach, the interlayer dynamic interaction will exceed a certain threshold, which becomes sufficient to rapidly synchronize the motion of magnetic solitons and balance the spin current. Two solitons thereby get trapped in a stationary position see Figs. 3(e) and 3(f)]. This dynamic region of soliton immobilization is henceforth referred to as the locking region. These simulation results in the wider range of J' are summarized in Fig. 3(g), which clearly shows the decoupling-to-unlocking-to-locking

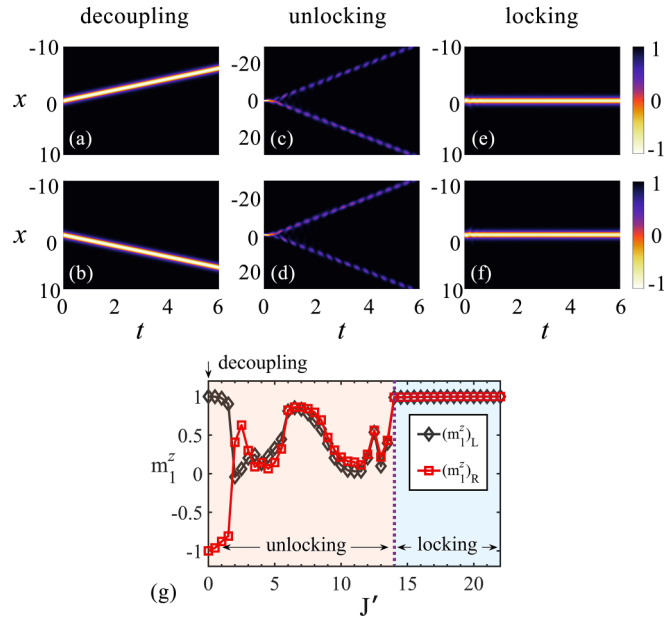

FIG. 3. The decoupling, unlocking, and locking regions of magnetic soliton motion. (a), (b) Propagations of m_1^z and m_2^z with dimensionless coupling strength $J' = 0$. (c), (d) Propagations of m_1^z and m_2^z with dimensionless coupling strength $J' = 10$. (e), (f) Propagations of m_1^z and m_2^z with dimensionless coupling strength $J' = 15$. (g) Phase diagram for the tristate transition by adjusting the interlayer coupling strength.

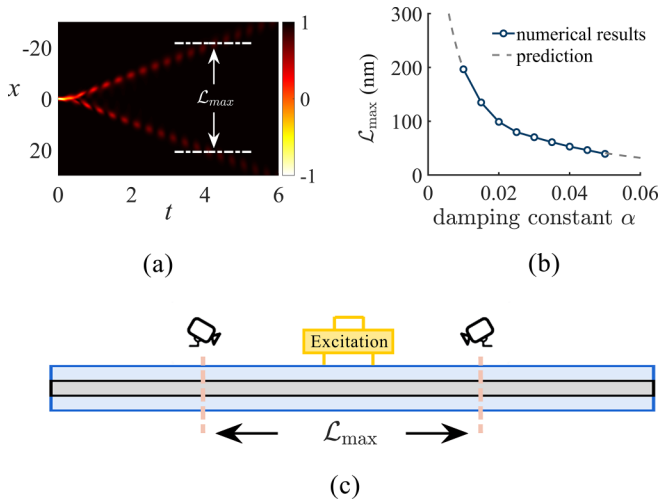

FIG. 4. The effect of Gilbert damping on the motion of magnetic soliton in unlocking phase. (a) Propagations of m_1^z with dimensionless coupling strength $J' = 10$, damping constant $\alpha = 0.05$, $\mathcal{L}_{\max}$ represents the maximum distance at which the signal attenuates to an unrecognizable state. (b) Dependence of the maximum distance $\mathcal{L}_{\max}$ for damping constant α. (c) Sketch of maximum separation distance between identifiable magnetic soliton signals.

transition. The black and red lines in the figure represent the minimum values of soliton signals received by the signal-receiving devices placed at both ends of the first layer FM under different coupling strengths.

The different behaviors of magnetic solitons in FM bilayers under varying coupling strengths inspire us to design a simple prototype observing the tristates transition experimentally [55,56]. Placing signal receptors on either side of the first FM layer, we can infer the separation between the two ferromagnetic layers based on the signals received. When they are considerably distant, only one side of the receptor can detect the magnetic soliton signal. As the two ferromagnetic layers come into closer proximity, both sides of the receptor can receive the magnetic soliton signal. However, when the two ferromagnetic layers are in close vicinity, neither side of the receptor registers the magnetic soliton signal. In practical applications, the signal attenuation caused by Gilbert damping in ferromagnetic materials must be considered. Through numerical simulation, we find that the damping effect has a significant impact on the magnetic solitons in the unlocking state. Figure 4(a) shows the propagation of magnetic solitons in the unlocking state in the upper FM layer with Gilbert-damping constant $\alpha_1 = 0.05$, where $\mathcal{L}_{\max}$ represents the maximum distance at which the signal attenuates to an unrecognizable state (assuming that the m^z component is greater than 0.8). The dependence of $\mathcal{L}_{\max}$ on the damping constant α for the FM layer is shown in Fig. 4(b). It can be observed that opting for materials featuring low damping coefficients can significantly increase the separation between signal receivers.

IV. DISCUSSION AND CONCLUSION

To sum up, we have derived a model at a small amplitude approximation to describe the nonlinear dynamics of magnetization in a bilayer ferromagnetic system. When the intermediate layer takes a characteristic thickness (i.e., 2 nm), $s = J/2K$ for the system here, and the dynamic interaction coupling parameter and magnetic anisotropy are taken as $2\ \mathrm{mJ/m^2}$ and $5 \times 10^5\ \mathrm{J/m^3}$, it is possible to introduce a gauge transformation to transform the equation into a fully integrable constant coefficient Manakov system. The first-order and second-order nondegenerate magnetic soliton solutions are obtained, as well as their respective stability regions. The numerical simulation results of magnetic soliton transmission are well consistent with the predictions given by linear stability. These theoretical and numerical results confirm the existence of stable one-dimensional magnetic soliton pairs in magnetic bilayer systems. To generate such magnetic solitons in a F/N/F bilayer system, the magnetization texture based on the above magnetic soliton solution must be manufactured into the two ferromagnetic layers. These excited solitons can be achieved, for example, by a local magnetic filed or spin-polarized electric currents.

On the other hand, the intensity of the interlayer long-range dynamic interaction, induced by adiabatic spin pump, can be tailored by manipulating the spacing between the two FM layers. Through the manipulation of the intermediate layer's thickness, we unveiled three distinct transport states of magnetic solitons: soliton decoupling, unlocking, and locking. With a gradual increment in dynamic interactions, we demonstrated the progression of magnetic soliton motion from decoupling to unlocking, and ultimately to locking. It is noted that the dynamic exchange coupling strength J is related to the thickness of the spacing layer. We postulate an inverse square root relationship between the two parameters [19,57,58], i.e., $J \propto 1/\sqrt{s}$. Through calculations based on the parameters we have considered, it is determined that when the thickness of the intermediate layer is less than 0.45 nm, magnetic solitons initiate a transition towards the locking state. Note that the thickness of this transition is related to the selection of ferromagnetic layer and insulating spacer layer materials. In this paper, we primarily reference the physical parameters of the Co/Cu/Co structure. Nevertheless, it is worth noting that this specific material is not a prerequisite for generating vector magnetic solitons in magnetic bilayers. In fact, we can substitute the ferromagnetic layer with $Fe_xNi_{1-x}Br_2$ [59] or some magnetic garnets with strong easy-axis anisotropy, and utilize Pt in lieu of the nonmagnetic interlayer to enhance the coupling strength [22]. Moreover, various material characteristics, such as the saturation magnetization strength M_s and the interface coupling of synthetic ferromagnetic layers, can be controlled within the realm of advanced materials manufacturing and deposition technologies. This enables the creation of magnetic bilayer systems capable of supporting nondegenerate magnetic solitons with varying thicknesses.

Finally, we examine the impact of Gilbert damping in different ferromagnetic materials on this transitional process. Our findings reveal that damping predominantly results in the attenuation of magnetic solitons in the unlocking state. Furthermore, we have established a correlation between the damping coefficient and the maximum separation distance between distinguishable magnetic soliton signals. These findings present new possibilities for developing spintronic devices for logic computing based on magnetic solitons, and

have ignited extensive research on these systems to refine their design according to specific application requirements.

ACKNOWLEDGMENTS

The authors thank Profs. H. Yu and C. Liu for their helpful discussions. This work was supported by the National Natural Science Foundation of China (Grants No. 12275213, No. 12174306, and No. 12247103), and Natural Science Basic Research Program of Shaanxi (Grants No. 2023-JC-JQ-02 and No. 2021JCW-19).

APPENDIX: PERTURBED PROPAGATION IN 2D MAGNETIC BILAYERS

In real-world scenarios, ferromagnetic thin-film materials possess finite width. Thus it is meaningful to evaluate the perturbed propagation of our obtained magnetic soliton pair in 2D thin films. We performed numerical simulations to test the stability of stable and unstable soliton solution in the 2D medium. Encouragingly, the numerical results closely align with the theoretical predictions, as illustrated in Fig. 5. The top four panels depict the perturbed propagation of a stable soliton pair in the magnetic bilayer films, where the shapes of the soliton pair are well maintained. Conversely, the bottom four panels show the perturbed propagation of an unstable magnetic soliton pair. During this process, the magnetic soliton pairs become unstable and eventually split after a certain transmission distance. It is conceivable that when the thin films become sufficiently narrow, they can be approximated as a one-dimensional scenario.

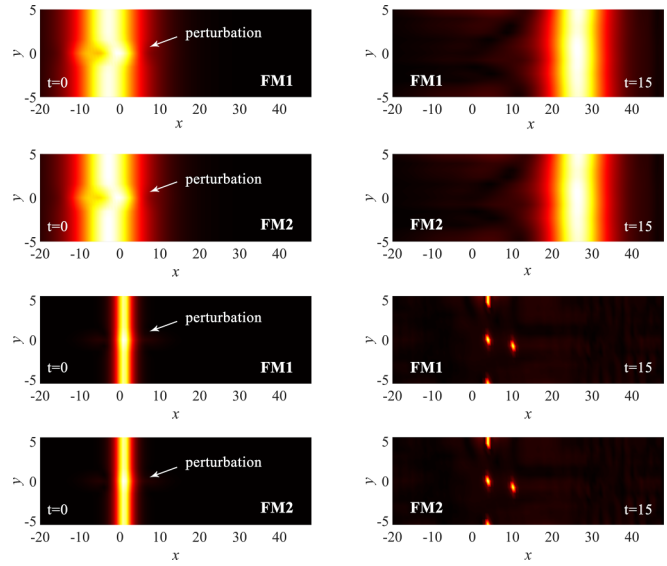

FIG. 5. Stable and unstable evolution of magnetic solitons in bilayer systems under 2D perturbations $\Psi_p = 0.1 \cdot \exp(-(x/8)^2 - y^2)$. The parameters of stable magnetic soliton are chosen as $\alpha_{11} = 0.44 + 0.51i, \alpha_{12} = 0.43 + 0.59i, k_1 = l_1 = 0.2$. The parameters of unstable magnetic soliton are chosen as $\alpha_{11} = 0.44 + 0.51i, \alpha_{12} = 0.43 + 0.59i, k_1 = l_1 = 0.8$.

[1] A. M. Kosevich, B. Ivanov, and A. Kovalev, Magnetic solitons, Phys. Rep. **194**, 117 (1990).
[2] H. Wang, R. Yuan, Y. Zhou, Y. Zhang, J. Chen, S. Liu, H. Jia, D. Yu, J.-P. Ansermet, C. Song *et al.*, Long-Distance coherent propagation of high-velocity antiferromagnetic spin waves, Phys. Rev. Lett. **130**, 096701 (2023).
[3] C. Liu, J. Chen, T. Liu, F. Heimbach, H. Yu, Y. Xiao, J. Hu, M. Liu, H. Chang, T. Stueckler *et al.*, Long-distance propagation of short-wavelength spin waves, Nat. Commun. **9**, 738 (2018).
[4] C.-Z. Li, A.-Q. Wang, C. Li, W.-Z. Zheng, A. Brinkman, D.-P. Yu, and Z.-M. Liao, Topological transition of superconductivity in dirac semimetal nanowire josephson junctions, Phys. Rev. Lett. **126**, 027001 (2021).
[5] J. Lan, W. Yu, J. Xiao *et al.*, Geometric magnonics with chiral magnetic domain walls, Phys. Rev. B **103**, 214407 (2021).
[6] M. Ohkuma, M. Mito, Y. Kousaka, T. Tajiri, J. Akimitsu, J. Kishine, and K. Inoue, Soliton locking phenomenon over finite magnetic field region in the monoaxial chiral magnet $CrNb_3S_6$, Appl. Phys. Lett. **117**, 232403 (2020).
[7] X. Zhang, Y. Zhou, K. M. Song, T.-E. Park, J. Xia, M. Ezawa, X. Liu, W. Zhao, G. Zhao, and S. Woo, Skyrmion-electronics: writing, deleting, reading and processing magnetic skyrmions toward spintronic applications, J. Phys.: Condens. Matter **32**, 143001 (2020).
[8] K. Gu, Y. Guan, B. K. Hazra, H. Deniz, A. Migliorini, W. Zhang, and S. S. Parkin, Three-dimensional racetrack memory devices designed from freestanding magnetic heterostructures, Nat. Nanotechnol. **17**, 1065 (2022).
[9] H. Zhang, W. Kang, L. Wang, K. L. Wang, and W. Zhao, Stateful reconfigurable logic via a single-voltage-gated spin hall-effect driven magnetic tunnel junction in a spintronic memory, IEEE Trans. Electron Devices **64**, 4295 (2017).
[10] Y. Tserkovnyak, A. Brataas, G. E. W. Bauer, and B. I. Halperin, Nonlocal magnetization dynamics in ferromagnetic heterostructures, Rev. Mod. Phys. **77**, 1375 (2005).
[11] S. Klingler, V. Amin, S. Geprägs, K. Ganzhorn, H. Maier-Flaig, M. Althammer, H. Huebl, R. Gross, R. D. McMichael, M. D. Stiles *et al.*, Spin-torque excitation of perpendicular standing spin waves in coupled YIG/Co heterostructures, Phys. Rev. Lett. **120**, 127201 (2018).
[12] R. Gallardo, T. Schneider, A. Chaurasiya, A. Oelschlägel, S. Arekapudi, A. Roldán-Molina, R. Hübner, K. Lenz, A. Barman, J. Fassbender *et al.*, Reconfigurable spin-wave nonreciprocity induced by dipolar interaction in a coupled ferromagnetic bilayer, Phys. Rev. Appl. **12**, 034012 (2019).
[13] J. C. Slonczewski, Current-driven excitation of magnetic multilayers, J. Magn. Magn. Mater. **159**, L1 (1996).
[14] D. Apalkov, A. Khvalkovskiy, S. Watts, V. Nikitin, X. Tang, D. Lottis, K. Moon, X. Luo, E. Chen, A. Ong *et al.*, Spin-transfer torque magnetic random access memory (STT-MRAM), J. Emerg. Technol. Comput. Syst. **9**, 1 (2013).
[15] Z. Li and S. Zhang, Domain-wall dynamics driven by adiabatic spin-transfer torques, Phys. Rev. B **70**, 024417 (2004).
[16] Z. Li and S. Zhang, Domain-wall dynamics and spin-wave excitations with spin-transfer torques, Phys. Rev. Lett. **92**, 207203 (2004).

[17] Y. Liu, W. Hou, X. Han, and J. Zang, Three-dimensional dynamics of a magnetic hopfion driven by spin transfer torque, Phys. Rev. Lett. **124**, 127204 (2020).

[18] B. Heinrich, Y. Tserkovnyak, G. Woltersdorf, A. Brataas, R. Urban, and G. E. Bauer, Dynamic exchange coupling in magnetic bilayers, Phys. Rev. Lett. **90**, 187601 (2003).

[19] Y. Li, W. Cao, V. P. Amin, Z. Zhang, J. Gibbons, J. Sklenar, J. Pearson, P. M. Haney, M. D. Stiles, W. E. Bailey *et al.*, Coherent spin pumping in a strongly coupled magnon-magnon hybrid system, Phys. Rev. Lett. **124**, 117202 (2020).

[20] J. Zhou, S. Saha, Z. Luo, E. Kirk, V. Scagnoli, and L. J. Heyderman, Ultrafast laser induced precessional dynamics in antiferromagnetically coupled ferromagnetic thin films, Phys. Rev. B **101**, 214434 (2020).

[21] H. Yazdi, G. Ghasemi, M. Mohseni, and M. Mohseni, Tuning the dynamics of magnetic droplet solitons using dipolar interactions, Phys. Rev. B **103**, 024441 (2021).

[22] X. Zhang, Y. Zhou, and M. Ezawa, Magnetic bilayer-skyrmions without skyrmion Hall effect, Nat. Commun. **7**, 10293 (2016).

[23] T. Xu, J. Liu, X. Zhang, Q. Zhang, H.-A. Zhou, Y. Dong, P. Gargiani, M. Valvidares, Y. Zhou, and W. Jiang, Systematic control of the interlayer exchange coupling in perpendicularly magnetized synthetic antiferromagnets, Phys. Rev. Appl. **18**, 054051 (2022).

[24] S. Nadj-Perge, I. K. Drozdov, J. Li, H. Chen, S. Jeon, J. Seo, A. H. MacDonald, B. A. Bernevig, and A. Yazdani, Observation of Majorana fermions in ferromagnetic atomic chains on a superconductor, Science **346**, 602 (2014).

[25] R. Cai, I. Žutić, and W. Han, Superconductor/ferromagnet heterostructures: A platform for superconducting spintronics and quantum computation, Adv. Quantum Technol. **6**, 2200080 (2023).

[26] L. Sheng, M. Elyasi, J. Chen, W. He, Y. Wang, H. Wang, H. Feng, Y. Zhang, I. Medlej, S. Liu *et al.*, Nonlocal detection of interlayer three-magnon coupling, Phys. Rev. Lett. **130**, 046701 (2023).

[27] J. Linder and J. W. Robinson, Superconducting spintronics, Nat. Phys. **11**, 307 (2015).

[28] Q. Yang, R. Mishra, Y. Cen, G. Shi, R. Sharma, X. Fong, and H. Yang, Spintronic integrate-fire-reset neuron with stochasticity for neuromorphic computing, Nano Lett. **22**, 8437 (2022).

[29] D. Wang, R. Tang, H. Lin, L. Liu, N. Xu, Y. Sun, X. Zhao, Z. Wang, D. Wang, Z. Mai *et al.*, Spintronic leaky-integrate-fire spiking neurons with self-reset and winner-takes-all for neuromorphic computing, Nat. Commun. **14**, 1068 (2023).

[30] T. L. Gilbert, A phenomenological theory of damping in ferromagnetic materials, IEEE Trans. Magn. **40**, 3443 (2004).

[31] A. S. Kovalev, A. M. Kosevich, and K. V. Maslov, Magnetic vortex-topological soliton in a ferromagnet with an easy-axis anisotropy, Pis'ma Zh. Eksp. Teor. Fiz. **30**, 321 (1979) [JETP Lett. **30**, 296 (1979)].

[32] E. Iacocca, T. J. Silva, and M. A. Hoefer, Breaking of Galilean invariance in the hydrodynamic formulation of ferromagnetic thin films, Phys. Rev. Lett. **118**, 017203 (2017).

[33] Z. Chen, X. Zhang, Y. Zhou, and Q. Shao, Skyrmion dynamics in the presence of deformation, Phys. Rev. Appl. **17**, L011002 (2022).

[34] B. A. Kalinikos, N. G. Kovshikov, and C. E. Patton, Self-generation of microwave magnetic envelope soliton trains in yttrium iron garnet thin films, Phys. Rev. Lett. **80**, 4301 (1998).

[35] M. Bauer, O. Büttner, S. Demokritov, B. Hillebrands, V. Grimalsky, Y. Rapoport, and A. Slavin, Observation of spatiotemporal self-focusing of spin waves in magnetic films, Phys. Rev. Lett. **81**, 3769 (1998).

[36] A. N. Slavin, S. O. Demokritov, and B. Hillebrands, in *Spin Dynamics in Confined Magnetic Structures I* (Springer, 2001) pp. 35–64

[37] B. Ivanov and A. Kosevich, Bound states of a large number of magnons in a ferromagnet with a single-ion anisotropy, Sov. Phys. JETP **45**, 1050 (1977).

[38] M. M. Bogdan and A. S. Kovalev, Exact multisoliton solution of one-dimensional Landau-Lifshitz equations for an anisotropic ferromagnet, JETP Lett. **31**, 424 (1980).

[39] A. M. Kosevich, M. P. Voronov, and I. V. Manzhos, Nonlinear collective excitations in an easy plane magnet, Zh. Eksp. Teor. Fiz. **84**, 148 (1983).

[40] A. Kosevich, V. Gann, A. Zhukov, and V. Voronov, Magnetic soliton motion in a nonuniform magnetic field, J. Exp. Theor. Phys. **87**, 401 (1998).

[41] J. Tan, Z.-H. Deng, T. Wu, and B. Tang, Propagation and interaction of magnetic solitons in a ferromagnetic thin film with the interfacial Dzyaloshinskii-Moriya interaction, J. Magn. Magn. Mater. **475**, 445 (2019).

[42] C. Liu, S. Wu, J. Zhang, J. Chen, J. Ding, J. Ma, Y. Zhang, Y. Sun, S. Tu, H. Wang *et al.*, Current-controlled propagation of spin waves in antiparallel, coupled domains, Nat. Nanotechnol. **14**, 691 (2019).

[43] H. Yuan, Y. Cao, A. Kamra, R. A. Duine, and P. Yan, Quantum magnonics: When magnon spintronics meets quantum information science, Phys. Rep. **965**, 1 (2022).

[44] J. Wang, J. Ma, H. Huang, J. Ma, H. M. Jafri, Y. Fan, H. Yang, Y. Wang, M. Chen, D. Liu *et al.*, Ferroelectric domain-wall logic units, Nat. Commun. **13**, 3255 (2022).

[45] L. Shen, Y. Zhou, and K. Shen, Programmable skyrmion-based logic gates in a single nanotrack, Phys. Rev. B **107**, 054437 (2023).

[46] S. Stalin, R. Ramakrishnan, M. Senthilvelan, and M. Lakshmanan, Nondegenerate solitons in Manakov system, Phys. Rev. Lett. **122**, 043901 (2019).

[47] R. Ramakrishnan, S. Stalin, and M. Lakshmanan, Nondegenerate solitons and their collisions in Manakov systems, Phys. Rev. E **102**, 042212 (2020).

[48] S. Stalin, R. Ramakrishnan, and M. Lakshmanan, Dynamics of nondegenerate vector solitons in a long-wave–short-wave resonance interaction system, Phys. Rev. E **105**, 044203 (2022).

[49] Y.-H. Qin, L.-C. Zhao, and L. Ling, Nondegenerate bound-state solitons in multicomponent Bose-Einstein condensates, Phys. Rev. E **100**, 022212 (2019).

[50] See Supplemental Material at http://link.aps.org/supplemental/10.1103/PhysRevB.109.014414 for the details on the derivation of first- and second-order nondegenerate magnetic solitons, the associated linear stability analysis, and an exploration of the robustness of degenerate magnetic solitons with respect to variations in the intermediate layer thickness. The Supplemental Material also contains Refs. [47,48,51].

[51] J. Yang, *Nonlinear Waves in Integrable and Nonintegrable Systems* (SIAM, 2010).

[52] S. Saha, J. Agudo-Canalejo, and R. Golestanian, Scalar active mixtures: the nonreciprocal Cahn-Hilliard model, Phys. Rev. X **10**, 041009 (2020).

[53] Z. Chen and J. Zeng, Two-dimensional optical gap solitons and vortices in a coherent atomic ensemble loaded on optical lattices, Commun. Nonline. Sci. Numerical Simulation **102**, 105911 (2021).

[54] V. E. Zakharov and E. A. Kuznetsov, Solitons and collapses: two evolution scenarios of nonlinear wave systems, Phys. Usp. **55**, 535 (2012).

[55] A. V. Chumak, P. Kabos, M. Wu, C. Abert, C. Adelmann, A. Adeyeye, J. Åkerman, F. G. Aliev, A. Anane, A. Awad *et al.*, Advances in magnetics roadmap on spin-wave computing, IEEE Trans. Magn. **58**, 1 (2022).

[56] A. Mahmoud, F. Ciubotaru, F. Vanderveken, A. V. Chumak, S. Hamdioui, C. Adelmann, and S. Cotofana, Introduction to spin wave computing, J. Appl. Phys. **128**, 161101 (2020).

[57] M. D. Stiles, Interlayer exchange coupling, J. Magn. Magn. Mater. **200**, 322 (1999).

[58] P. Bruno, Theory of interlayer magnetic coupling, Phys. Rev. B **52**, 411 (1995).

[59] S. Hayami, S.-Z. Lin, and C. D. Batista, Bubble and skyrmion crystals in frustrated magnets with easy-axis anisotropy, Phys. Rev. B **93**, 184413 (2016).